

We are IntechOpen, the world's leading publisher of Open Access books Built by scientists, for scientists

4,600

Open access books available

120,000

International authors and editors

135M

Downloads

Our authors are among the

154

Countries delivered to

TOP 1%

most cited scientists

12.2%

Contributors from top 500 universities



WEB OF SCIENCE™

Selection of our books indexed in the Book Citation Index
in Web of Science™ Core Collection (BKCI)

Interested in publishing with us?
Contact book.department@intechopen.com

Numbers displayed above are based on latest data collected.
For more information visit www.intechopen.com



Reflectarray Pattern Optimization for Advanced Wireless Communications

Daniel Rodríguez Prado, Manuel Arrebola and Marcos Rodríguez Pino

Abstract

A framework for the design and optimization of large dual-linear polarized, shaped-beam reflectarrays for advanced wireless communications is presented. The methodology is based on the generalized intersection approach (IA) algorithm for both phase-only synthesis (POS) and direct optimization of the reflectarray layout, as well as on the use of a method of moments in the spectral domain assuming local periodicity. A thorough description of the design and optimization procedures is provided. To demonstrate the capabilities of the proposed framework, two examples are considered. The first example is a shaped-beam reflectarray for future 5G base stations working in the millimeter waveband, radiating a sectored-beam pattern in azimuth and squared-cosecant pattern in elevation to provide constant power in the coverage area. The second example is a very large contoured-beam reflectarray for direct-to-home (DTH) broadcasting based on real mission requirements with Southern Asia coverage.

Keywords: array pattern synthesis, reflectarrays, optimization, wireless communications, 5G, base station, space communications, shaped-beam, contoured-beam, generalized intersection approach

1. Introduction

Wireless communication technologies have experienced a constant and rapid development over the past few decades. This has resulted in communication systems that need to fulfill increasing tighter requirements with the goal of improving their performance and quality. In particular, future developments and integration of 5G technologies for terrestrial and space communications [1] represent a great challenge. Specifically, the antenna is an important subsystem for wireless communications, since it is the device that converts the guided waves into propagating waves in free space and vice versa. Different parameters of the antenna may be optimized depending on the application, such as size, radiation pattern, matching, etc. In many cases, a shaped-beam pattern is necessary to adequately redirect power to the desired area. For instance, direct-to-home (DTH) applications need a contoured-beam footprint to match some specific geographic area on the surface of the Earth [2]. Also, an interesting feature for base stations for wireless communications is to provide constant power over a certain angular range. This may be achieved with a shaped-beam

squared-cosecant pattern [3]. Traditionally, shaped parabolic reflectors or phased arrays have been employed for these applications [2, 3]. However, shaped parabolic reflectors are bulky and expensive to manufacture, while phased arrays require complex feeding networks which introduce high losses. Nonetheless, with the popularization of the microstrip technology, reflectarray antennas have become a potential substitute to parabolic reflector dishes and phased arrays.

The concept of reflectarray antenna was first introduced in 1963 [4] as a type of antenna that combines the simplicity of reflectors and the versatility of arrays, using waveguides as the reflecting element. This resulted in a bulky and expensive structure. However, reflectarrays were not widely studied until the development of low-profile printed antennas in the 1980s, when the printed planar reflectarray was developed [5]. It consists of an array of radiating elements that are spatially fed by a primary feed, which is usually a horn antenna. Its working principle is based on altering the properties of the electromagnetic field impinging from the feed. By adjusting the dimensions of the reflectarray elements, a phase shift is introduced in the impinging field [6], allowing to obtain the desired radiation pattern.

Although designing reflectarrays for high-gain pencil beam patterns at a certain direction may be achieved with analytical equations [5], the synthesis of noncanonical beams is a challenging task and requires the use of an optimization algorithm, especially in cases with tight requirements, such as space applications [2]. Since reflectarrays are usually comprised of hundreds or even thousands of elements, the employed algorithm must be computationally efficient. Until recently, the dominant approach was the phase-only synthesis (POS) [5], which employs a simplified analysis of the unit cell. This results in an extremely efficient synthesis [7–9] but has no control over the cross-polarization performance. The first approach to the crosspolar direct optimization of reflectarray antennas was presented in [10], using a method of moments based on local periodicity (MoM-LP) for the analysis of the unit cell. However, the algorithm was slow and only handled 1 polarization and small reflectarrays (225 elements). Other approaches for the minimization of the crosspolar component of the far field include a proper arrangement of the elements [11] and the minimization of the undesired tangential field adjusting the dimensions of the element [12] or through rotation [13]. These techniques are faster, but they work at the element level and thus provide suboptimal results.

In this chapter, we present a general framework for the efficient and accurate pattern optimization of reflectarray antennas for advanced wireless communications, including copolar and crosspolar specifications. It is based on the use of the generalized intersection approach (IA) algorithm [14] for the optimization and a MoM-LP [15] for the accurate characterization of the reflectarray unit cell. The design procedure is divided in several stages. First, a phase-only synthesis (POS) is carried out, to efficiently obtain the desired copolar pattern. Then, by using a zero-finding routine and the MoM-LP, the layout of the reflectarray is obtained adjusting the dimensions of each unit cell. Finally, an optional stage to improve the cross-polarization performance may be carried out. It employs the MoM-LP directly in the optimization loop to accurately characterize the crosspolar pattern. Both the POS and direct layout optimization are carried out with the generalized IA, demonstrating the versatility of the algorithm. Two relevant examples are provided to demonstrate the capabilities of the proposed framework. First, a shaped-beam reflectarray for future 5G base stations at millimeter waveband is proposed. It radiates a sectored-beam pattern in azimuth and a squared-cosecant pattern in elevation. The second example is a very large contoured-beam, spaceborne reflectarray for direct-to-home (DTH) broadcasting based on a real space mission.

The rest of the chapter is divided as follows. Section 2 introduces the optimization framework based on the generalized IA algorithm. Section 3 describes the

design and optimization methodology using the generalized IA. Section 4 contains the results regarding the two reflectarray designs for advanced wireless communications. Finally, Section 5 contains the conclusions.

2. Optimization framework for electrically large reflectarrays

2.1 Pattern requirements in the optimization procedure

Before describing in detail the optimization algorithm, we will establish the different pattern requirements that can be imposed in the optimization procedure and how they are implemented in the generalized IA. For the case of radiation pattern optimization, the requirements may be imposed in the copolar and crosspolar components. When performing a POS, only copolar requirements are considered due to the simplifications in the analysis of the unit cell [9]. However, a direct optimization of the layout may consider both copolar and crosspolar requirements. In the generalized IA, the copolar requirements are given by means of two mask templates, which impose the minimum (T_{\min}) and maximum (T_{\max}) values that the far field must achieve. Thus, if G_{cp} is the copolar gain, it should fulfil

$$T_{\min}(u, v) \leq G_{\text{cp}}(u, v) \leq T_{\max}(u, v), \quad (1)$$

where $u = \sin \theta \cos \varphi$ and $v = \sin \theta \sin \varphi$ are the angular coordinates where the far field is computed. **Figure 1** shows an example of typical copolar requirement templates for a squared-cosecant pattern and a sectored-beam pattern in a plane, where T_{\min} and T_{\max} are the minimum and maximum specifications between which the copolar pattern must lie. Alternatively, these requirements can be provided in terms of minimum gain and maximum ripple.

On the other hand, there are several methodologies to implement crosspolar requirements. A typical approach is to minimize the crosspolar far field component by means of templates [16], similarly to the procedure followed with the copolar pattern. However, the crosspolar pattern does not need a lower bound in the optimization. Thus, only the maximum mask T_{\max}^{xp} is needed in this case, where the superscript indicates that the mask is applied to the crosspolar pattern, fulfilling

$$G_{\text{xp}}(u, v) \leq T_{\max}^{\text{xp}}(u, v). \quad (2)$$

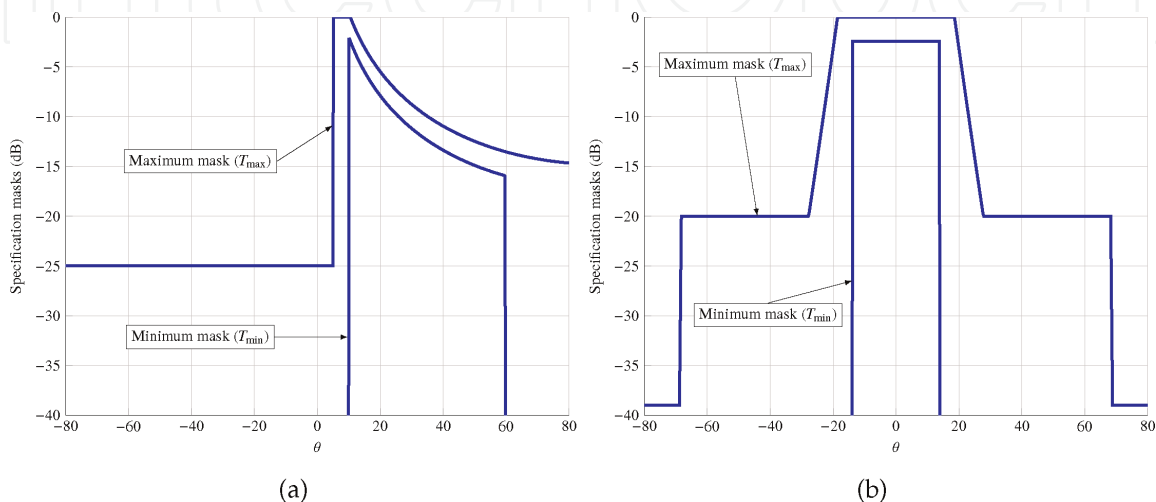


Figure 1. Typical requirement templates for (a) squared-cosecant pattern and (b) sectored-beam pattern.

However, there are applications in which the figure of merit for cross-polarization performance is not the crosspolar pattern. In particular, some space missions [2] give the requirements for the crosspolar discrimination (XPD) and/or crosspolar isolation (XPI).

The XPD is defined for a certain coverage zone as the difference (in logarithmic scale) point by point of the copolar gain and the crosspolar gain. Mathematically it is expressed as

$$\text{XPD}(u, v) = G_{\text{cp}}(u, v) - G_{\text{xp}}(u, v), \quad (u, v) \in \Omega, \quad (3)$$

where Ω is the coverage zone, XPD is in dB and G_{cp} and G_{xp} are in dBi. Usually, the minimum XPD is considered, since it is the value limiting the XPD performance in the coverage zone:

$$\text{XPD}_{\min} = \min \{ \text{XPD}(u, v) \}, \quad (u, v) \in \Omega. \quad (4)$$

Similarly, the XPI is defined for a certain coverage zone as the difference (in logarithmic scale) of the minimum copolar gain and the maximum crosspolar gain:

$$\text{XPI} = G_{\text{cp}, \min}(u, v) - G_{\text{xp}, \max}(u, v), \quad (u, v) \in \Omega, \quad (5)$$

where XPI is in dB and $G_{\text{cp}, \min}$ and $G_{\text{xp}, \max}$ are in dBi. Notice that, unlike the XPD, the XPI is defined as a single value for a given coverage area. Also, the XPI is a stricter parameter than the XPD. **Figure 2** shows graphically how the XPD and XPI are defined.

The optimization procedure should maximize the XPD_{\min} and/or XPI. Thus, if $T_{\text{XPD}_{\min}}$ and T_{XPI} are the minimum requirement templates for XPD_{\min} and XPI, respectively, they should fulfill the following condition:

$$T_{\text{XPD}_{\min}} \leq \text{XPD}_{\min}, \quad (6)$$

$$T_{\text{XPI}} \leq \text{XPI}. \quad (7)$$

2.2 Generalized intersection approach

The framework for the optimization of the radiation pattern of reflectarray antennas is based on the generalized intersection approach (IA) [4]. A flowchart of the algorithm is shown in **Figure 3**. It is an iterative algorithm which performs two operations at each iteration i on the tangential field:

$$\vec{E}_{\text{ref}, i+1} = \mathcal{B} \left[\mathcal{F} \left(\vec{E}_{\text{ref}, i} \right) \right], \quad (8)$$

where \vec{E}_{ref} is the tangential field on the reflectarray surface, calculated as

$$\vec{E}_{\text{ref}}(x_l, y_l) = \mathbf{R}^l \vec{E}_{\text{inc}}(x_l, y_l), \quad (9)$$

where (x_l, y_l) are the coordinates of the centre of the reflectarray element l , \vec{E}_{inc} is the fixed incident field impinging from the feed and

$$\mathbf{R}^l = \begin{pmatrix} \rho_{xx}^l & \rho_{xy}^l \\ \rho_{yx}^l & \rho_{yy}^l \end{pmatrix} \quad (10)$$

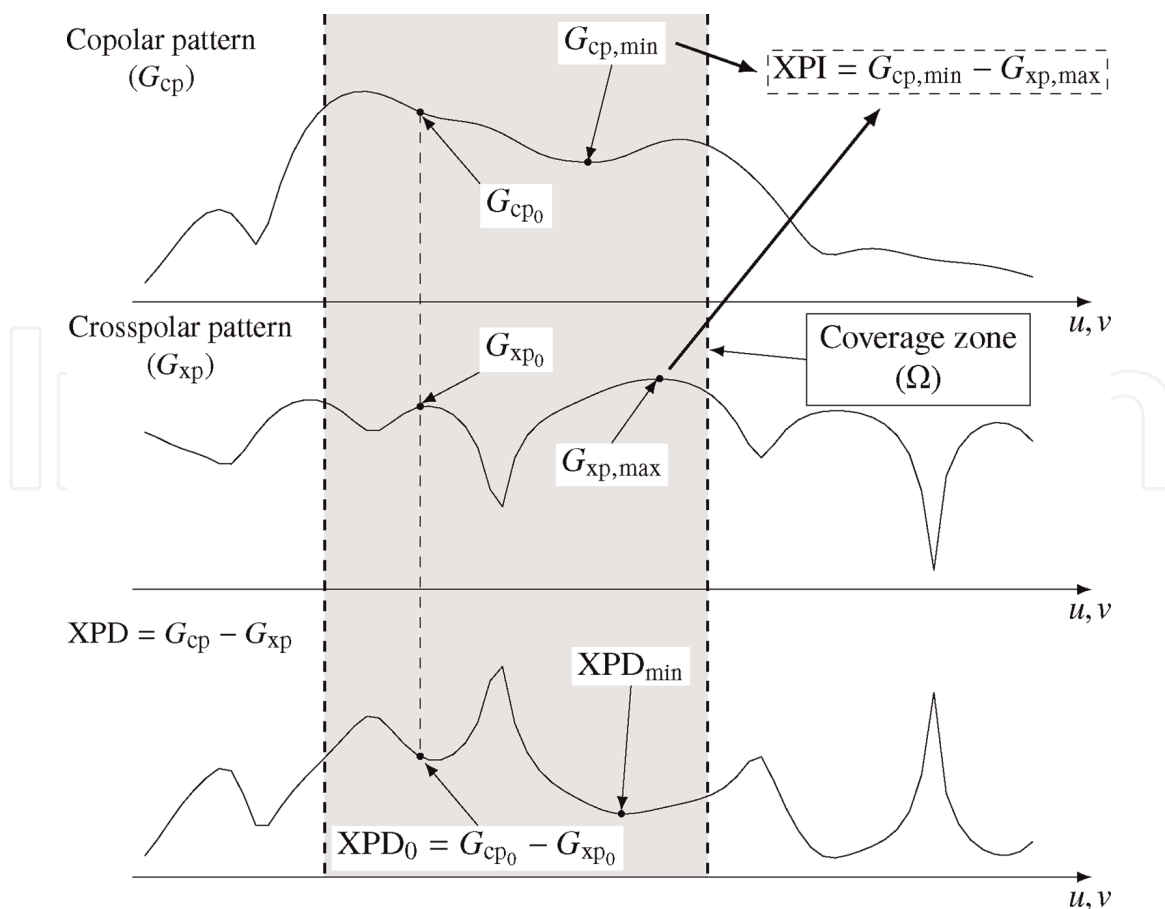


Figure 2. Graphical definition of the parameters for co- and cross-polarization performance: The crosspolar discrimination (XPD), which is defined point by point as the difference between the copolar gain and the crosspolar gain, and the crosspolar isolation (XPI), which is defined for the coverage zone as the difference between the minimum copolar gain and the maximum crosspolar gain. The copolar and crosspolar patterns are in dBi, while the XPD and the XPI are in dB.

is the matrix of reflection coefficients which define the electromagnetic behaviour of the unit cell. These coefficients are complex numbers and are computed by a full-wave analysis tool assuming local periodicity [5]. ρ_{xx} and ρ_{yy} are known as the direct coefficients, while ρ_{xy} and ρ_{yx} are known as the cross-coefficients. In addition, the copolar pattern mainly depends on the direct coefficients phase, and the crosspolar pattern depends on all coefficients.

In (8), \mathcal{F} is the forward projector. As shown in **Figure 3**, it is divided into two steps. First, starting from the tangential field, which depends on the optimizing variables, either the phases of the direct coefficients in a phase-only synthesis or the reflectarray element geometry in the case of a direct optimization, it computes the current far field radiated by the reflectarray. In its second step, it trims the far field according to the specification masks. For the power pattern synthesis, the specifications may be given in gain. Thus, if G is the current gain of the reflectarray and G' the trimmed gain, then

$$G'(u, v) = \begin{cases} T_{\max}(u, v), & T_{\max}(u, v) < G(u, v) \\ T_{\min}(u, v), & G(u, v) < T_{\min}(u, v) \\ G(u, v), & \text{otherwise.} \end{cases} \quad (11)$$

This operation is also applied to the crosspolar pattern when performing a direct optimization of the reflectarray layout. If the cross-polarization performance is

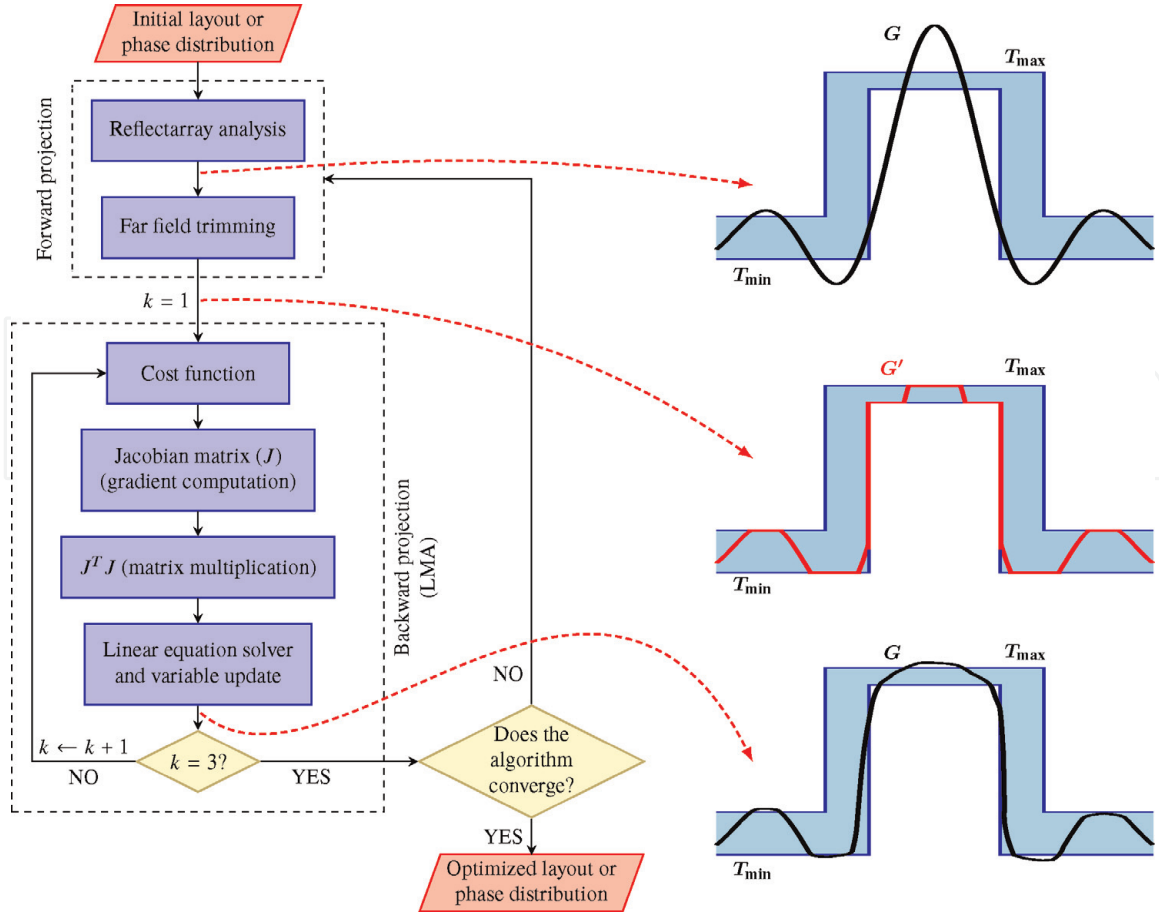


Figure 3. Flowchart of the generalized intersection approach algorithm as applied to the far field in gain.

improved by means of the XPD_{\min} or XPI optimization, a similar expression to Eq. (11) is used but only taking into account the minimum masks, as in Eqs. (6) and (7).

The second operation of the generalized IA, denoted by \mathcal{B} in Eq. (8), is the backward projector. It minimizes the distance between the trimmed gain and the current gain radiated by the antenna (see **Figure 3**), obtaining a reflected tangential field that generates a radiation pattern that is closer to fulfil specifications:

$$\vec{E}_{\text{ref}, i+1} = \mathcal{B}[\mathcal{F}(\vec{E}_{\text{ref}, i})] = \min \text{dist}[G_i, \mathcal{F}(\vec{E}_{\text{ref}, i})]. \quad (12)$$

The latter operation is performed by a general minimizing algorithm [14]. In addition, as a distance definition, we employ the Euclidean norm for square-integrable functions [8], which is implemented by the weighted Euclidean metric:

$$d_i = \text{dist}^2(\mathcal{F}(\vec{E}_{\text{ref}, i}), G_i(u, v)) = \iint_{\Lambda} w(u, v)(G'_i(u, v) - G_i(uv))^2 du dv, \quad (13)$$

where it was taken into account that the result of the forward projection is the trimmed gain in Eq. (11); $w(u, v)$ is a weighting function; and Λ is a subset of the visible region ($u^2 + v^2 \leq 1$) where the radiation pattern is optimized. The integral in Eq. (13) can be approximated by a sum for the points (u, v) that belong to Λ :

$$d_i = \sum_{u, v \in \Lambda} \left[\sqrt{w(u, v) \Delta u \Delta v} (G'_i(u, v) - G_i(uv)) \right]^2. \quad (14)$$

This sum can be minimized by the Levenberg-Marquardt algorithm (LMA) [9].

Finally, the generalized IA can be applied to perform a phase-only synthesis (POS), where the optimizing variables are the phase shift introduced by each reflectarray element corresponding to the phases of the direct coefficients in Eq. (10), or a direct layout optimization, where the optimizing variables are the geometrical features of the unit cell.

3. Design and optimization methodology

This section briefly describes the design methodology employing the optimization framework presented in the previous section. It is applied to a reflectarray in single-offset configuration, as shown in **Figure 4**. The procedure is divided into three stages: first, a phase-only synthesis to obtain the desired radiation pattern; then, a design procedure to adjust the element dimensions yielding a reflectarray layout; and the last and optional stage is the optimization of the cross-polarization performance of the reflectarray antenna.

3.1 Phase-only synthesis for the copolar pattern

The first step in the design of a shaped-beam reflectarray antenna is a phase-only synthesis (POS). The aim of the POS is to obtain a phase-shift distribution that generates the desired shaped radiation pattern, which in general cannot be obtained through analytical means since that approach presents some limitations [9]. Since we are interested in dual-linear polarized reflectarrays, two phase-shift distributions are necessary, one for each linear polarization. In addition, the generalized IA is a local search algorithm. Thus, a good starting point is of utmost importance.

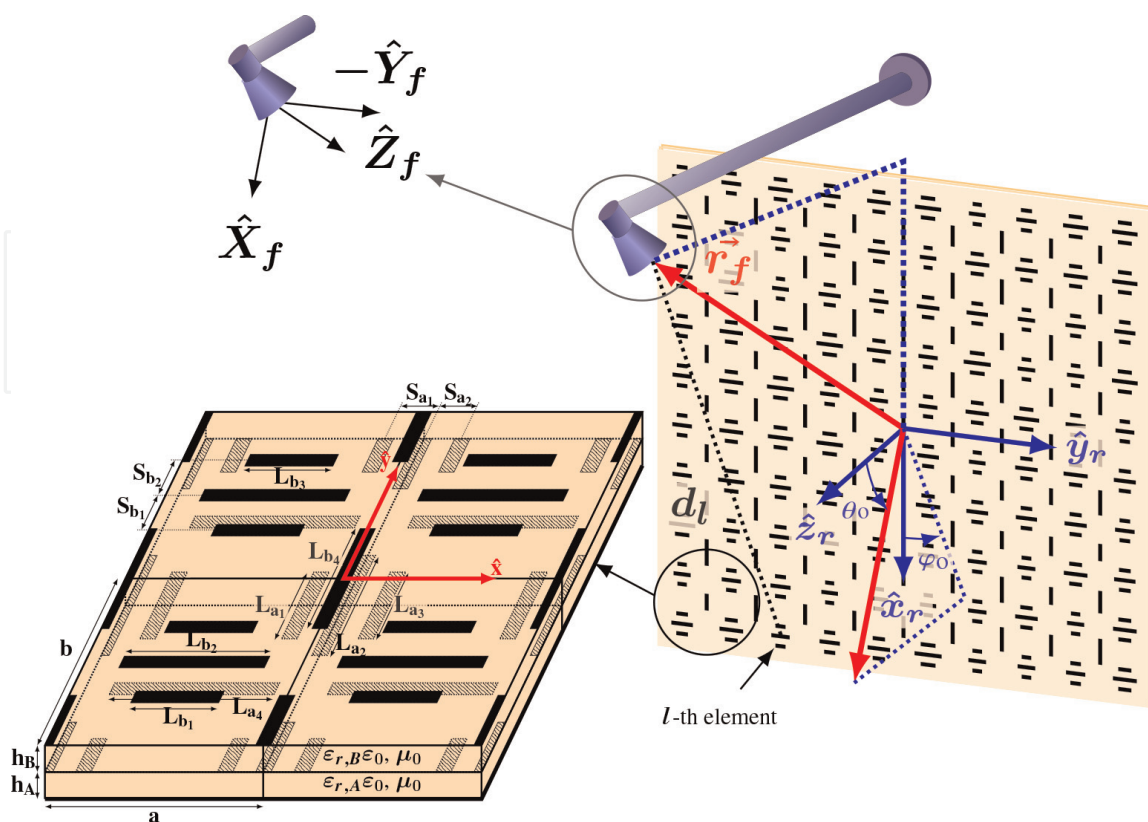


Figure 4. Diagram of the planar reflectarray antenna optics and the considered unit cell based on two sets of parallel and coplanar dipoles. © 2018 IEEE. Reprinted, with permission, from [17].

It has been demonstrated that a properly focused pattern is sufficient for the POS [7]. In that case, the initial phase distribution for the POS may be obtained analytically [5]:

$$\angle\rho(x_l, y_l) = k_0(d_l - (x_l \cos \varphi_0 + y_l \sin \varphi_0) \sin \theta_0), \quad (15)$$

where $\angle\rho(x_l, y_l)$ is the phase of a direct reflection coefficient (ρ_{xx} or ρ_{yy} , for linear polarizations X and Y, respectively); d_l is the distance from the feed to the l th element (see **Figure 4**); and (θ_0, φ_0) is the pointing direction of the focused beam. The angle (θ_0, φ_0) is usually selected in a direction where the desired shaped beam has maximum gain.

Then, the generalized IA is employed to synthesize the desired pattern. For the POS, the elements are modelled as ideal phase shifters, in which there are no losses ($|\rho_{xx}| = |\rho_{yy}| = 1$) and no cross-polarization ($\rho_{xy} = \rho_{yx} = 0$). Thus, the matrix of reflection coefficients in (11) is simplified to

$$\mathbf{R}^l = \begin{pmatrix} \exp(j\phi_{xx}^l) & 0 \\ 0 & \exp(j\phi_{yy}^l) \end{pmatrix}, \quad (16)$$

where ϕ^l is the phase of the corresponding reflection coefficient. Thus, the optimizing variables are the phases of the direct coefficients. In addition, the POS is carried out in several steps, gradually increasing the number of optimizing variables as suggested in [14] to further improve the convergence of the algorithm. Once the desired phase-shift distributions are obtained, the following step is to obtain the reflectarray layout.

3.2 Obtaining a reflectarray layout from a phase-shift distribution

The procedure to obtain a reflectarray layout from the two phase-shift distributions obtained after the POS is summarized in the flowchart of **Figure 5**.

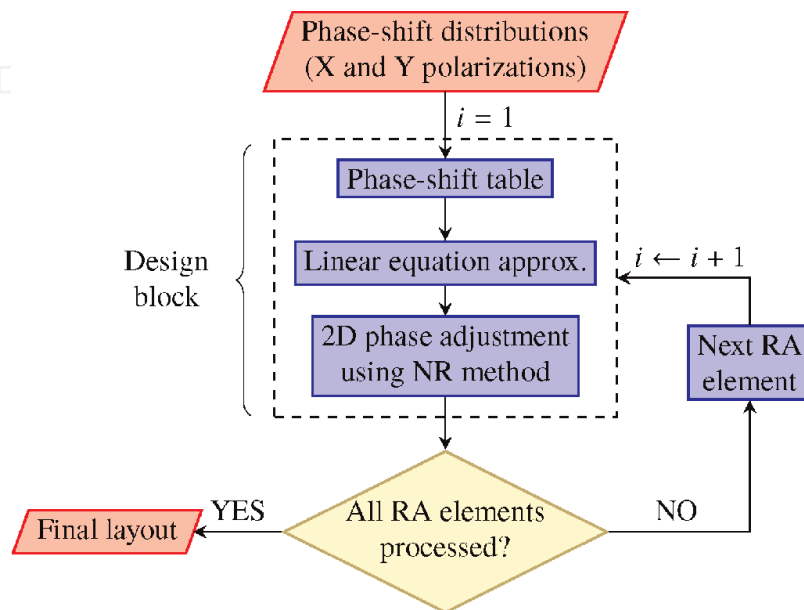


Figure 5. Flowchart of the procedure to obtain a reflectarray layout from the synthesized phase-shift distribution for two linear polarizations.

It requires the use of a full-wave technique based on local periodicity (FW-LP) to analyse the unit cell. Here, we employ the MoM-LP described in [18] to analyse the unit cell shown in **Figure 4**. In this step, a common procedure in the literature is to use a design curve obtained at normal incidence to seek the size of the reflectarray element that matches the required phase shift. However, it is recommended to consider the real angle of incidence to increase accuracy, especially for very large reflectarray antennas, since the phase shift varies with the angle of incidence [5].

This procedure is divided into three steps. Firstly, a phase-shift table is generated, increasing the size of the element (for instance, the patch size or dipole length) in little intervals. For the case at hand and using the unit cell based on two sets of parallel dipoles of **Figure 4**, two variables, T_x and T_y , are defined that allow to control the phase shift for linear polarizations X and Y, respectively. Thus, the phase-shift table is generated modifying at the same time T_x and T_y . Then, we select two sizes of the element that provide a phase shift a little above and below the exact value. This is done independently for the two linear polarizations. Next, a linear equation is used to approximate the value of the element size that provides the required phase shift. Finally, by using a zero-finding routine (for instance, the Newton-Raphson method as indicated in **Figure 5**), the exact value for both polarizations is sought at the same time, taking into account the coupling between polarizations. This is done for every reflectarray element, obtaining a layout which generates the desired radiation pattern obtained in the POS of the first stage.

3.3 Improvement of the cross-polarization performance through direct optimization

The third and final stage is optional and consists in improving the cross-polarization performance of the synthesized reflectarray by directly optimizing its layout using a FW-LP tool. This is especially important for applications with tight cross-polarization requirements, such as space missions [2], since the layout obtained in the previous stage most likely will only comply with copolar specifications. As a starting point, the layout obtained in the previous stage is employed. Also, the copolar specification masks are maintained to keep the copolar pattern within specifications while the cross-polarization performance is improved.

There are a number of approaches that can be followed in this stage depending on the application. A common approach in the literature is to directly minimize the crosspolar component of the far field [19, 20]. This is done by applying Eq. (2) for the crosspolar pattern masks in the forward projector of the generalized IA. Another approach is to impose Eqs. (6) and (7) in order to maximize the XPD_{min} or the XPI. This is especially convenient for space applications in which cross-polarization requirements are specified by those parameters [17].

Nevertheless, this stage requires the use of a FW-LP tool to obtain the full matrix of reflection coefficients in Eq. (10) in order to correctly characterize the crosspolar radiation pattern. Thus, the improvement in cross-polarization performance will be slower than the POS in the first stage.

4. Examples of application

Here, we present two examples of application of the optimization framework presented in the previous sections. First, a medium-sized reflectarray is designed to work in a base station for future 5G application in the millimeter band at 28 GHz. The second example is a very large contoured-beam reflectarray for

direct-to-home broadcasting in the Ku-band at 12.5 GHz, based on a real mission with Southern Asia coverage.

4.1 Reflectarray for 5G base station

4.1.1 Antenna specifications

For the first example, the considered reflectarray is circular and comprised of 912 unit cells (34 elements in the main axes). The periodicity is 5.36 mm in both axes, which is half a wavelength at the working frequency, 28 GHz, in order to avoid grating lobes [5]. The feed is placed at $(-79.3, 0.0, 200.2)$ mm with regard to the centre of the reflectarray (see **Figure 4**), and it is modelled as a $\cos^q \theta$ function, with $q = 20.6$, generating an illumination taper of -14.6 dB at the reflectarray edges.

The unit cell shown in **Figure 4** is used here. The separation between dipoles is set to $S_{a_i} = S_{b_i} = 1$ mm ($i = 1, 2$), while the width of all dipoles is set to 0.3 mm. Variables T_x and T_y are defined as

$$\begin{aligned} L_{a_4} = T_x; \quad L_{b_1} = L_{b_3} = 0.63T_x; \quad L_{b_2} = 0.93T_x \\ L_{b_4} = 0.95T_y; \quad L_{a_1} = L_{a_3} = 0.58T_y; \quad L_{a_2} = T_y. \end{aligned} \quad (17)$$

The same substrate is used in both layers of the unit cell, with $\epsilon_r = 3.0$ and $\tan \delta = 0.0010$, which corresponds to the commercially available Rogers R3003. In addition, the bottom layer has a height of $h_A = 30$ mil = 0.762 mm, while the top layer has a height of $h_B = 20$ mil = 0.508 mm. **Figure 6** presents a unit cell study at central frequency, showing the phase shift produced by the reflectarray element as well as the losses. As it can be seen, the angular stability is good while having low losses better than -0.3 dB. Furthermore, the phase shift provided by the unit cell is more than 720° , which is more than enough for a reflectarray design and subsequent optimization.

Regarding the far field specifications, the chosen pattern for the 5G base station has a 30° sectored beam in azimuth and a squared-cosecant beam in elevation to provide constant power flux in an elevation span of 50° .

4.1.2 Results of the antenna design

The starting point for the POS is a pencil beam pointing at $(\theta = 10.4^\circ, \varphi = 0)$. This direction corresponds to a region of the specification masks with high gain. To obtain this radiation pattern, the phase-shift distribution calculated with Eq. (15) is employed, and it is shown in **Figure 7a** for polarization X, that is, for the direct

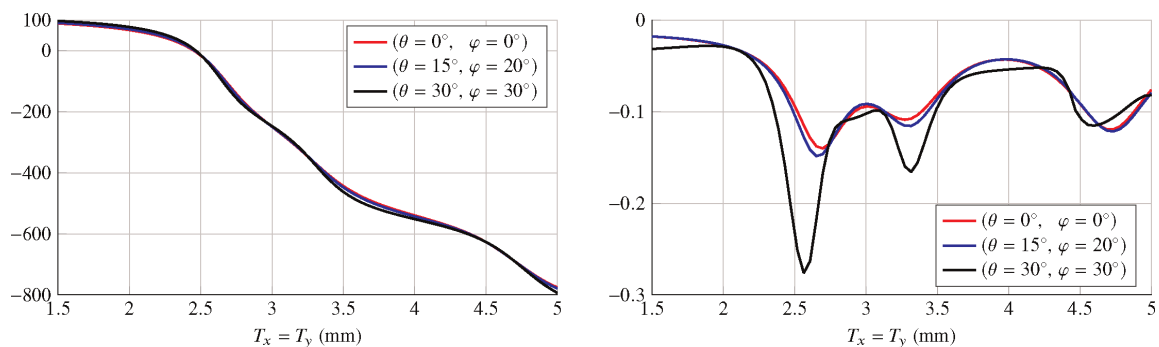


Figure 6. Unit cell study for the reflectarray for 5G base station at 28 GHz showing the phase shift (left) and the magnitude (right) for several angles of incidence. Unit cell presents a good angular stability with low losses.

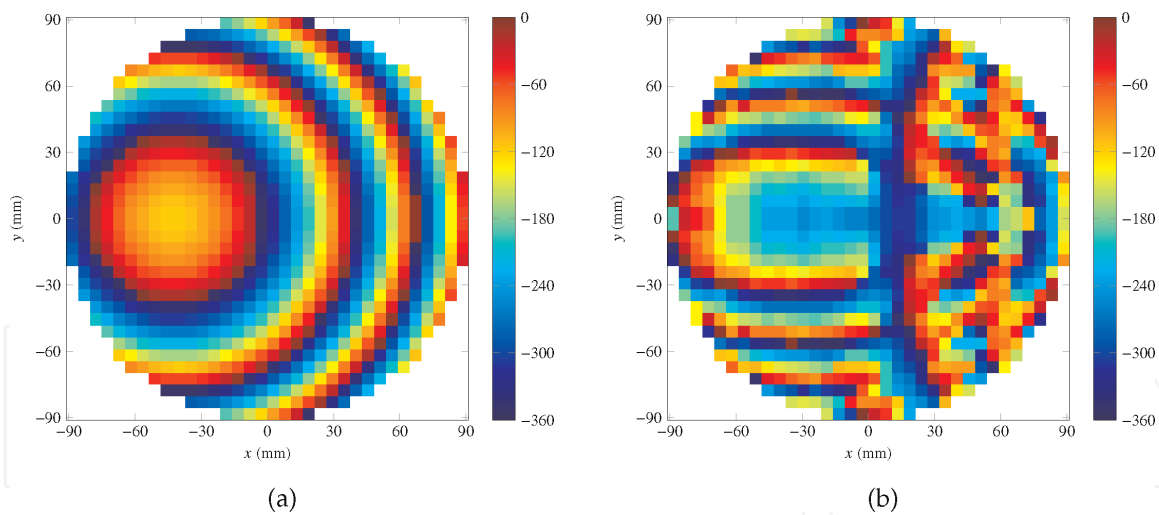


Figure 7.
 For polarization X: (a) starting phase distribution (in degrees) obtained with Eq. (15) for the POS and (b) synthesized phase distribution (in degrees) after the POS with the generalized IA.

reflection coefficient ρ_{xx} (the phase shift for polarization Y is the same). After the POS, the synthesized phase shift of **Figure 7b** is obtained, which generates the desired radiation pattern. Then, by using the procedure summarized in **Figure 5**, the reflectarray layout is found.

The obtained layout was simulated with a MoM-LP [18], and the resulting radiation pattern for polarization X is shown in **Figure 8**, where the copolar and crosspolar components of the far field are shown in the $u - v$ plane for the whole visible region. In this representation, it can be seen the sectored beam is along the v axis for constant u , while along u the squared-cosecant beam reduces the gain of the antenna from a maximum of 19.6 dBi to roughly 5 dB. This represents a dynamic range of almost 15 dB in which the shaped beam has to smoothly decrease over an angular span of 50° , making it challenging pattern to synthesize. In fact, it is very easy to obtain nulls in this region that penalize performance, even in simulations [21], and they have been avoided with success in the present example. Similar results were obtained for polarization Y.

On the other hand, **Figure 9** represents the main cuts in elevation and azimuth for both linear polarizations along with the mask requirements. Here, it can be

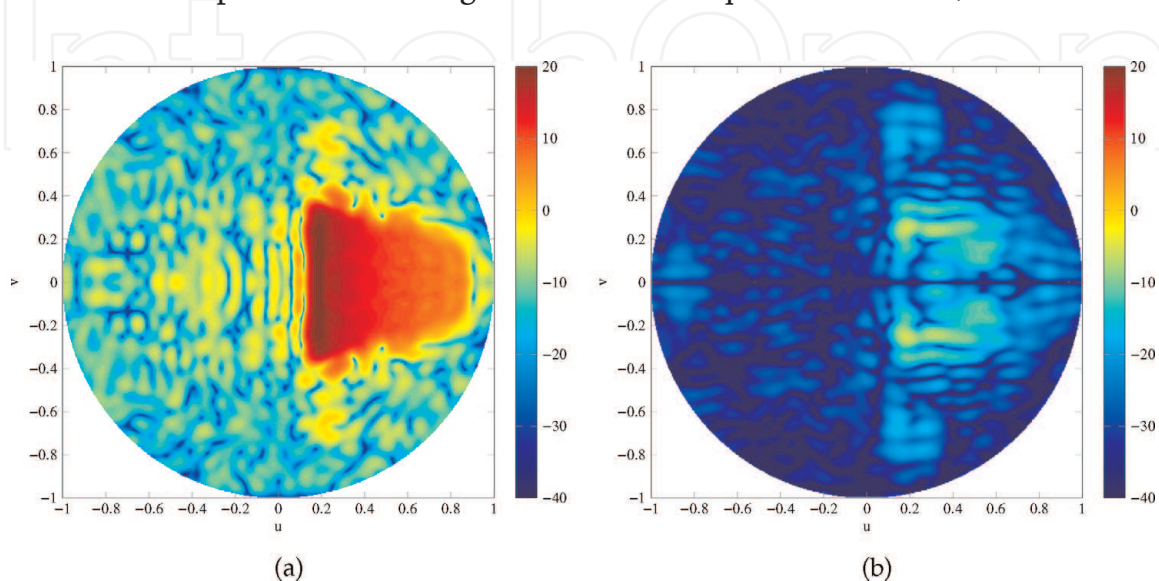


Figure 8.
 Radiation pattern in the whole visible region radiated by the reflectarray designed for a 5G base station for polarization X. (a) Copolar component of the far field. (b) Crosspolar component of the far field.

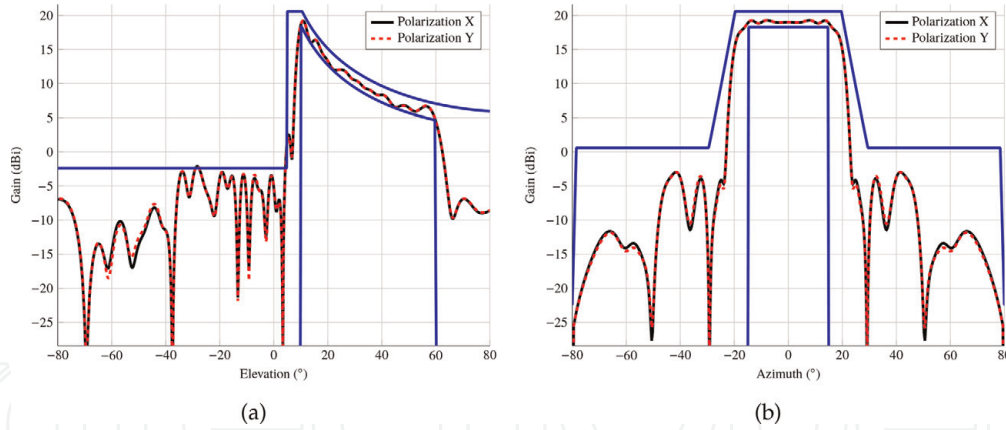


Figure 9. Main cuts for both linear polarizations in (a) elevation and (b) azimuth with the mask requirements for the reflectarray designed for a 5G base station.

better appreciated how the specifications are met, with side lobes lower than -2 dB, which represent a SLL better than 20 dB for this shaped pattern. In addition, **Figure 10** shows the radiation pattern in 3D perspective, along with a sketch of the reflectarray panel.

Regarding the cross-polarization performance, the initial design presents maximum crosspolar values of -6.1 and -6.8 dBi for polarizations X and Y, respectively, while the maximum copolar gain is 19.6 dBi for both polarizations. This gives a maximum copolar gain/maximum crosspolar gain ratio (CP_{max}/XP_{max} from here on) of 25.7 and 26.4 dB for polarizations X and Y, respectively. The following step will be to improve the ratio CP_{max}/XP_{max} by minimizing the crosspolar component of the far field while keeping the copolar pattern within specifications and maintaining the maximum copolar gain. To this end, a direct optimization layout will be performed using the generalized intersection approach. Now, the optimizing variables will be variables T_x and T_y as defined in Eq. (17), instead of the phases of the reflection coefficients. In addition, since the starting point already complies with the copolar requirements, all variables will be optimized at the same time.

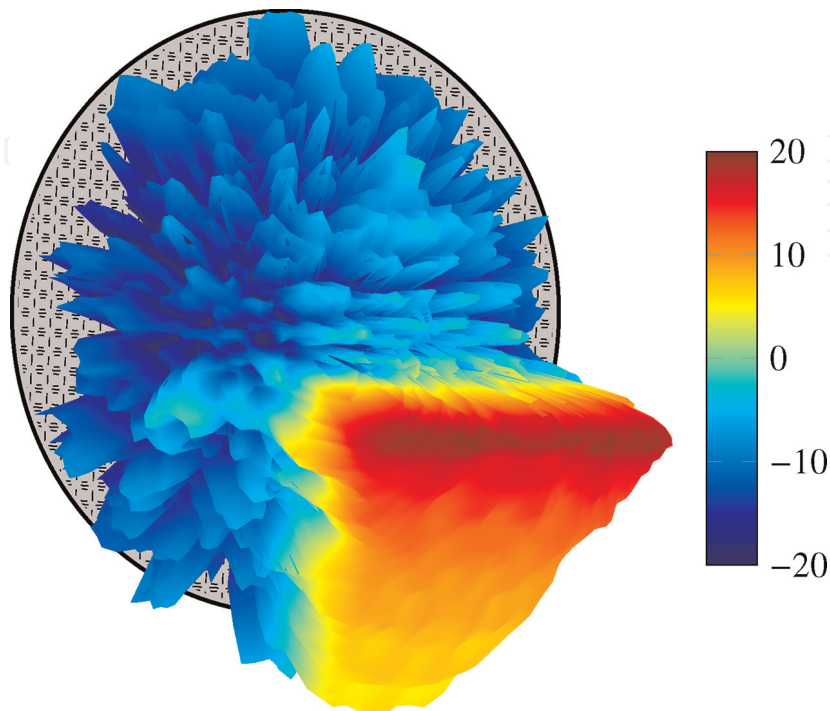


Figure 10. 3D representation of the copolar component of the radiation pattern for a 5G base station.

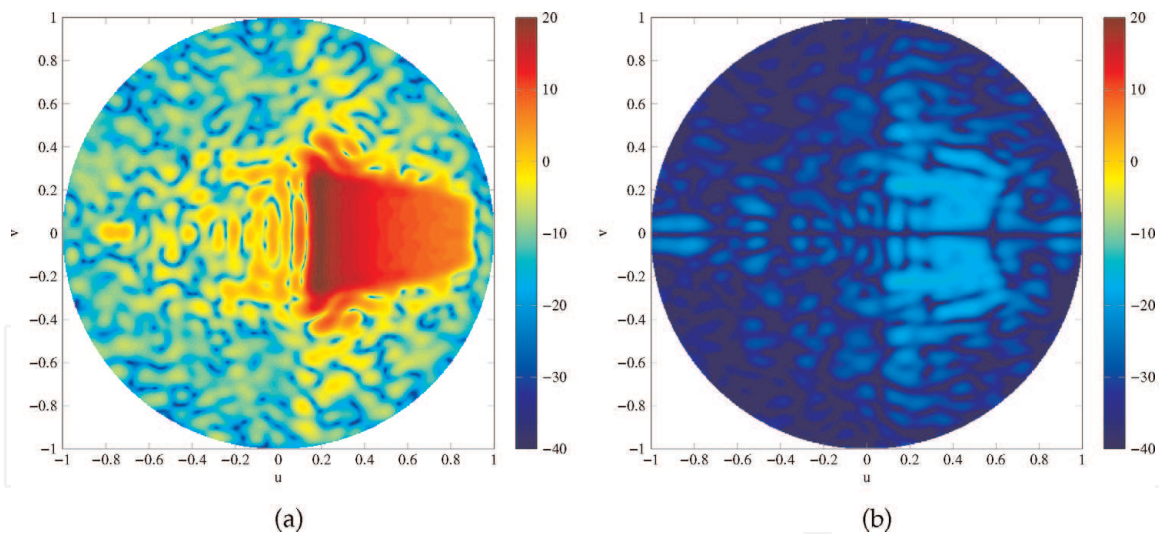


Figure 11. Radiation pattern in the whole visible region radiated by the reflectarray designed for 5G base station for polarization X after the optimization to improve the cross-polarization performance: (a) copolar component of the far field and (b) crosspolar component of the far field.

Thus, a total of 1824 variables will be considered. The copolar requirements are the same, while for the crosspolar pattern, a constant template T_{\max}^{XP} 40 dB below the maximum copolar gain is imposed for both linear polarizations. The goal is to minimize the crosspolar pattern as much as possible.

After the crosspolar optimization, the radiation pattern shown in **Figure 11** was obtained for polarization X. When compared with the far field of **Figure 8**, it can be seen how the crosspolar pattern maximum value has been considerably reduced while keeping the copolar pattern within specifications. In fact, the maximum copolar gain is now 19.7 dBi and 19.6 dBi for polarizations X and Y, respectively. At the same time, the maximum crosspolar values are -15.7 and -15.4 dBi, with $CP_{\max} - XP_{\max}$ values of 35.4 and 35.0 dB for polarizations X and Y, respectively. This represents an improvement of 9.7 and 8.6 dB for both linear polarizations. This information is summarized in **Table 1**. Finally, **Figure 12** shows the layout of the optimized reflectarray for both layers.

4.2 Reflectarray for direct-to-home satellite application

4.2.1 Antenna specifications

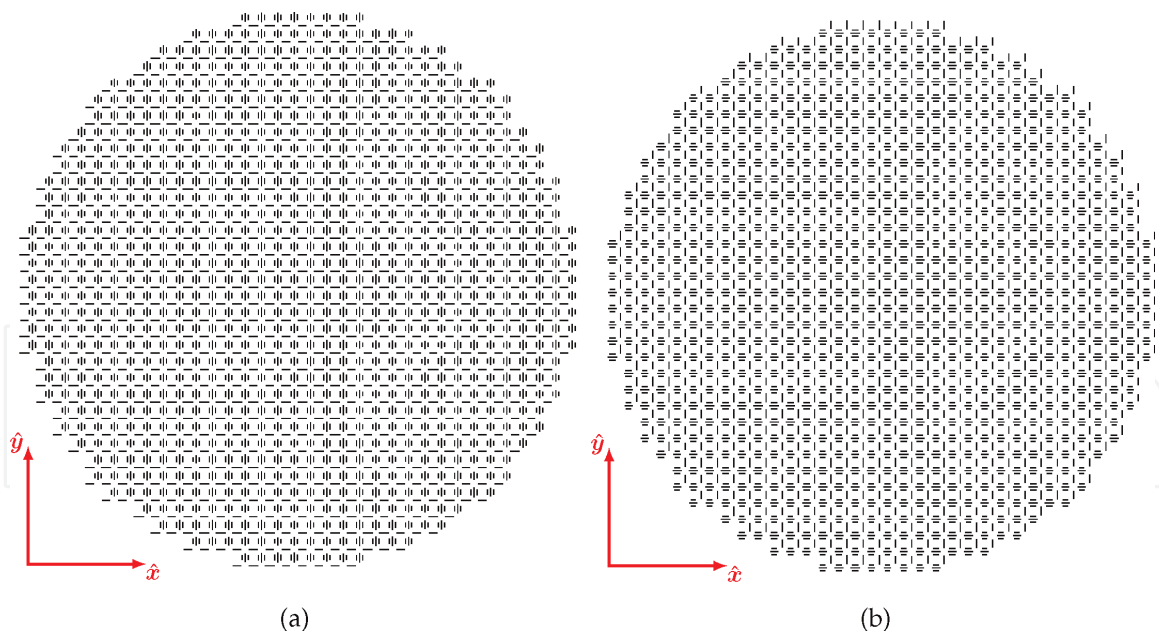
For the second example, an elliptical reflectarray with axes $1128 \text{ mm} \times 1080 \text{ mm}$ and comprised of 6640 elements, is considered. The reflectarray cells are arranged in a rectangular grid of 94×90 elements for polarization X and 93×89 elements for polarization Y, with a periodicity of 12 mm in both axes. The working frequency

	Polarization X			Polarization Y		
	CP_{\max}	XP_{\max}	$CP_{\max} - XP_{\max}$	CP_{\max}	XP_{\max}	$CP_{\max} - XP_{\max}$
Initial design	19.6	-6.12	25.7	19.6	-6.84	26.4
Optimized design	19.7	-15.75	35.4	19.6	-15.40	35.0

CP_{\max} and XP_{\max} are in dBi, while $CP_{\max} - XP_{\max}$ is in dB.

Table 1.

For the reflectarray for 5G base station, summary of the performance of the initial and optimized designs regarding the maximum copolar gain (CP_{\max}), the maximum crosspolar gain (XP_{\max}) and the difference between them ($CP_{\max} - XP_{\max}$) for both linear polarizations.

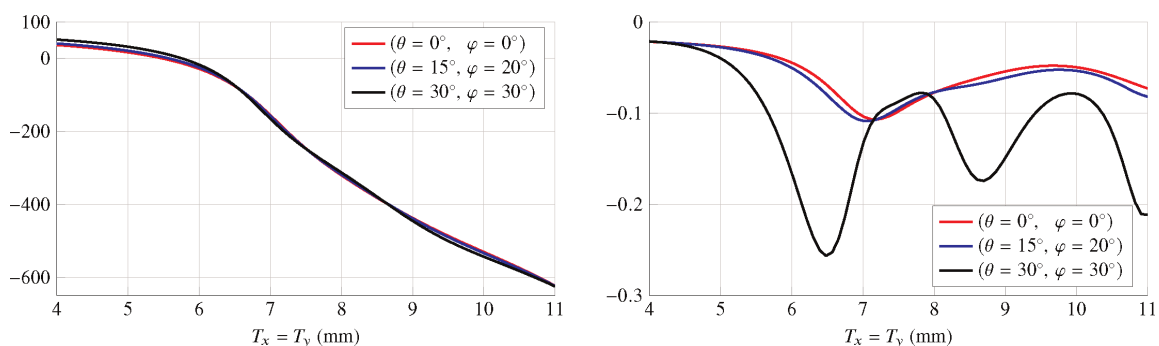

Figure 12.

Layout of the reflectarray designed for 5G base station that generates a radiation pattern with a 30° sectored beam in azimuth and a squared-cosecant beam in elevation: (a) bottom layer and (b) upper layer.

is 12.5 GHz. The feed is placed at $(-352.9, 0.0, 1061.7)$ mm with regard to the reflectarray centre and is modeled as a $\cos^q \theta$ with $q = 18$, which generates an illumination taper of -17.9 dB.

A similar unit cell as in the previous example is used with different dimensions and materials. The separation between dipoles is now set to $S_{a_i} = S_{b_i} = 2.5$ mm ($i = 1, 2$), while the width of all dipoles is set to 0.5 mm and T_x and T_y are defined in Eq. (17). Commercial substrates were chosen for both layers, the Arlon AD255C for the top layer, with $h_A = 2.363$ mm and $\epsilon_r = 2.17 - j0.0020$, and DiClad 880 for the bottom layer, with $h_B = 1.524$ mm and $\epsilon_r = 2.55 - j0.0036$. **Figure 13** presents a unit cell study at central frequency, showing the phase shift produced by the reflectarray element as well as the losses. As it can be seen, the angular stability is good while having low losses better than -0.3 dB. The phase shift provided by the cell is slightly larger than 600° .

Figure 14 shows the contour requirements for the Southern Asia mission, similar to that provided by the SES-12 satellite. Zone 1 includes India, Nepal, Bhutan, Bangladesh and Sri Lanka, while zone 2 includes Pakistan and Afghanistan. According to the official specifications [22], the satellite provides an EIRP of 52


Figure 13.

Unit cell study for the reflectarray for DTH at 12.5 GHz showing the phase shift (left) and the magnitude (right) for several angles of incidence. Unit cell presents a good angular stability with low losses while providing more than 600° of linear phase shift.

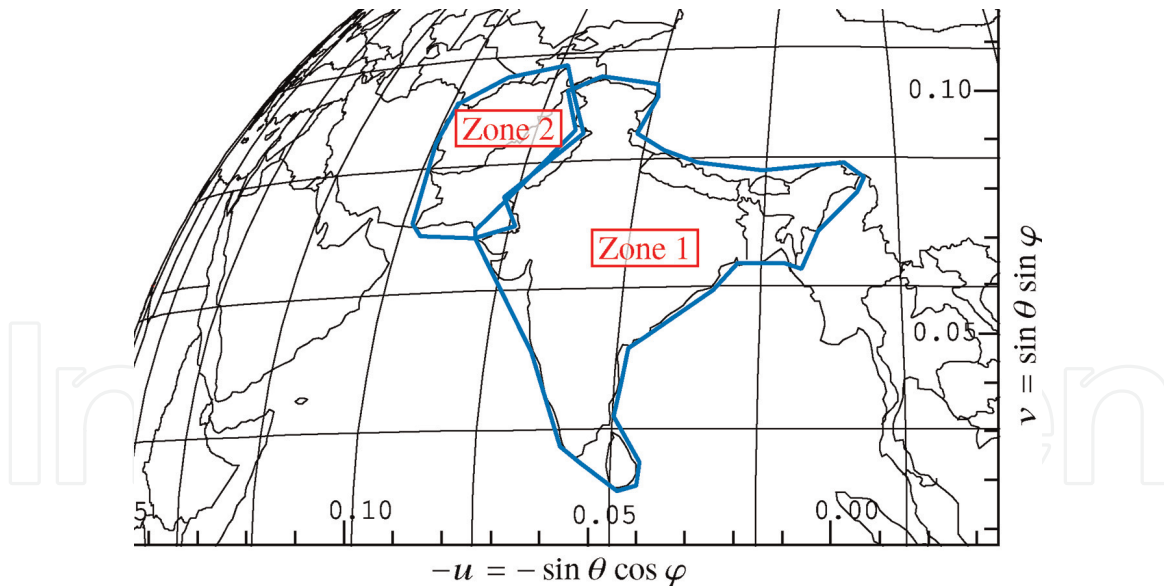


Figure 14. Footprint of the southern Asia coverage for direct-to-home broadcasting application. Zone 1 includes India, Nepal, Bhutan, Bangladesh and Sri Lanka, while zone 2 includes Pakistan and Afghanistan. This coverage mimics the one provided by the SES-12 satellite, placed in geostationary orbit at 95°E . (u, v) coordinates are in the satellite coordinate system.

dBW for zone 1 and 48 dBW for zone 2. The EIRP can be converted into gain using the following expression:

$$G(\text{dBi}) = \text{EIRP}(\text{dBW}) - P_t(\text{dBW}), \quad (18)$$

where P_t is the power of the transponder. Assuming $P_t = 150 \text{ W}$, it gives a gain specification of 30 dBi for zone 1 and 26 dBi for zone 2. In addition, the design process will take into account typical pointing errors (0.1° in roll and pitch and 0.5° in yaw). The design will be carried out in dual-linear polarization, imposing the same specifications in both polarizations.

4.2.2 Results of the antenna design

For the first step, a POS is carried out to obtain the desired copolar pattern in dual-linear polarization. **Figure 15a** shows the initial phase shift for the POS

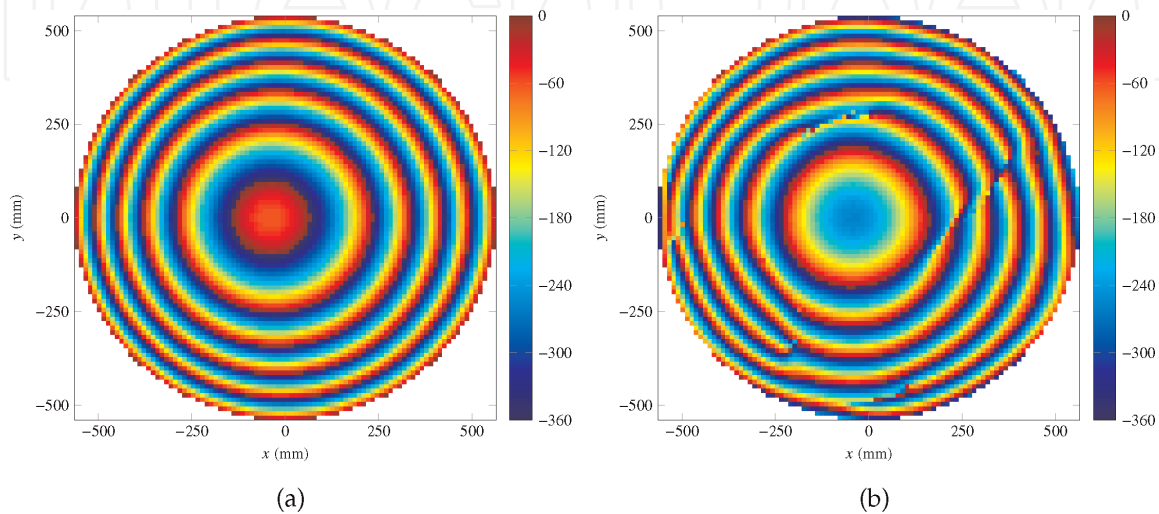


Figure 15. For polarization X: (a) starting phase distribution (in degrees) obtained with Eq. (15) for the POS and (b) synthesized phase distribution (in degrees) after the POS with the generalized IA.

obtained with Eq. (15). It generates a focused beam in the direction ($\theta = 16.5^\circ$, $\varphi = 0.0^\circ$), which corresponds to a high-gain area in India. After the synthesis, the phases shown in **Figure 15b** were obtained for polarization X. The phases for polarization Y are similar. Once the layout has been obtained, the radiation patterns were computed using a MoM-LP tool. The copolar and crosspolar components for this initial design are shown in **Figure 16** for polarization X. In this case, the minimum copolar gain is 31.5 and 28.6 dBi for zones 1 and 2, respectively. Similar results were obtained for polarization Y. Thus, the initial design complies with the requirements in both linear polarizations.

Space missions usually impose very stringent cross-polarization requirements in the form of crosspolar discrimination (XPD) and crosspolar isolation (XPI) for the transmit and receive bands, respectively. Notice that according to the definitions of minimum XPD in Eq. (4) and the XPI in Eq. (5), the XPI is a more stringent parameter than the XPD_{min} . The first row of **Table 2** shows the values of XPD_{min} and XPI for both coverage zones and polarizations. The initial design presents values of those parameters between 29.5 and 33.0 dB. The goal is thus to improve the cross-polarization performance of this reflectarray by performing a direct optimization of the layout. As in the previous case, T_x and T_y are considered as optimization variables. Thus, a total of 13,097 variables will be considered. In addition, instead of minimizing the crosspolar pattern as in the previous example, now the XPD_{min} and XPI will be optimized as detailed in [17]. To that end, minimum masks of 37 dB are imposed for both parameters. The goal is to increase as much as possible the XPD_{min} and XPI while keeping the minimum copolar gain for both coverage zones within specifications.

After the direct layout optimization, the cross-polarization performance of the reflectarray antenna significantly improved. The worst parameter is the XPI for zone 1 and polarization X, which has a value of 8 dB. It improved to 37.5 dB over the value for the initial design. The minimum improvement was 6 dB for the XPI for zone 1 and polarization X and XPD_{min} for zone 2 and polarization X. At the same time, the copolar minimum gain still complies with the specifications of 30 dBi for zone 1 and 26 dBi for zone 2. A summary of the performance of the initial and optimized layout may be found in **Table 2**. In addition, **Figure 17** shows the copolar and crosspolar pattern for polarization X of the optimized layout. Since the optimization has maximized the cross-polarization performance in the two coverage areas, the maximum crosspolar values are outside both of them.

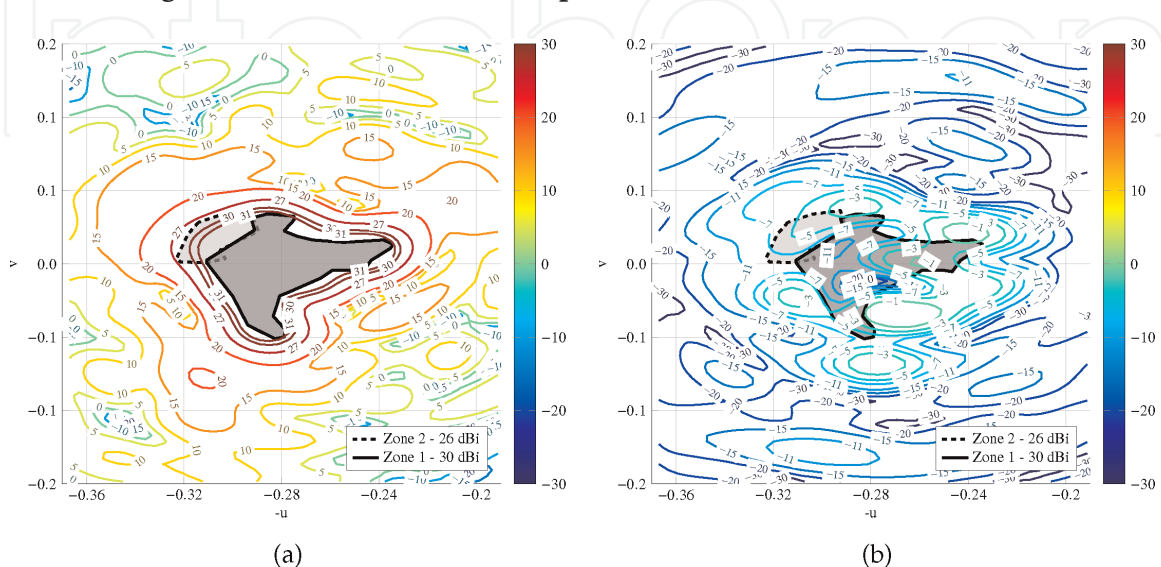


Figure 16. Radiation pattern of the initial layout with southern Asia coverage for polarization X: (a) copolar pattern and (b) crosspolar pattern.

	Zone 1						Zone 2					
	Polarization X			Polarization Y			Polarization X			Polarization Y		
	CP	XPD _{min}	XPI	CP	XPD _{min}	XPI	CP	XPD _{min}	XPI	CP	XPD _{min}	XPI
Initial design	31.52	32.50	32.08	31.36	30.51	29.56	28.63	32.99	31.13	28.91	31.76	29.87
Optimized design	30.07	38.99	38.11	30.04	39.77	37.51	29.15	39.01	37.53	29.17	39.79	38.23

CP is the minimum copolar gain in dBi in a coverage area, XPD_{min} is the minimum crosspolar discrimination in dB, and XPI is the crosspolar isolation in dB.

Table 2. For the reflectarray with southern Asia coverage, comparison of the performance of the initial design after the POS and the optimized layout for improved cross-polarization performance.

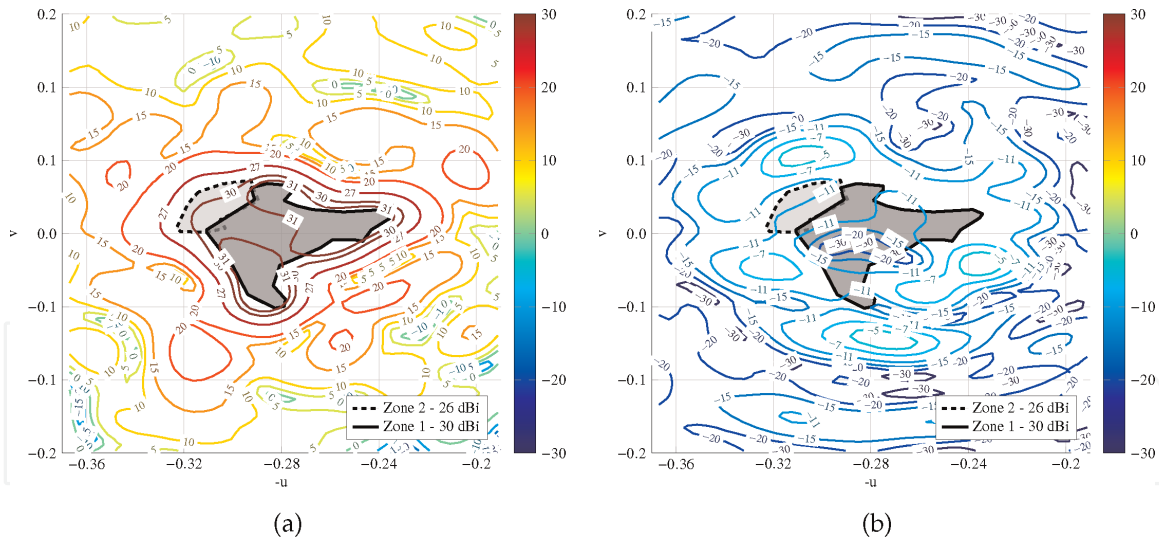


Figure 17. Radiation pattern of the optimized layout with southern Asia coverage for polarization X with improved cross-polarization performance: (a) copolar pattern and (b) crosspolar pattern.

Nevertheless, even its value has decreased, as it can be seen by comparing the crosspolar pattern of **Figures 16** and **17**.

5. Conclusions

A framework for the design and optimization of large dual-linear polarized reflectarray antennas has been presented. It is based on the generalized intersection approach (IA) algorithm, which is used for both a phase-only synthesis to obtain the initial design and a direct optimization of the reflectarray layout for a subsequent optimization of the cross-polarization performance. The IA employs the Levenberg-Marquardt algorithm in the backward projector and a method of moments based on local periodicity (MoM-LP) to accurately characterize the electromagnetic response of the unit cell.

In order to demonstrate the capabilities of the proposed framework, two examples for advanced wireless communication applications are provided. For the two designs, a unit cell that consists in two sets of parallel dipoles is employed. Each set of dipoles controls the phase shift of a linear polarization. The first example is a shaped-beam reflectarray for future 5G base stations, radiating a sectored beam in azimuth and a squared-cosecant beam in elevation. A circular reflectarray with a diameter of 182 mm and comprised of 912 elements was proposed. The shaped-beam reflectarray achieves a maximum gain of 19.6 dBi and a SLL better than 20 dB. In addition, the gain smoothly decreases its value in elevation a total of 15 dB over a tilt of 50° . This feature makes the synthesis of a squared-cosecant pattern a challenging task. Finally, the maximum value of the crosspolar pattern was reduced more than 8.5 dB for both linear polarizations after a direct layout optimization using MoM-LP directly in the optimization loop, while maintaining the copolar pattern within requirements.

The second example consists of a 1.1-metre reflectarray for direct-to-home (DTH) broadcasting application. A Southern Asia coverage footprint that emulates the requirements of the SES-12 satellite has been selected. This coverage presents two zones with different gain requirements: one comprising India, Nepal, Bhutan and Bangladesh with a 30 dBi of minimum copolar gain requirement and another for Pakistan and Afghanistan with a requirement of 26 dBi. After a phase-only

synthesis, the layout of the reflectarray was obtained using a zero-finding routine and simulated with a MoM-LP tool. The minimum copolar gain achieved in both linear polarizations is better than 31 dBi for zone 1, while it is better than 28 dBi for zone 2. Then, a direct optimization of the layout with MoM-LP was carried out to improve the cross-polarization performance. Both the minimum crosspolar discrimination and crosspolar isolation improved at least 6 dB for both zones and linear polarizations while keeping the minimum copolar gain within requirements.

The results shown here demonstrate the versatility of the proposed framework for the design and optimization of reflectarrays, as well as the feasibility of this type of antenna for advanced wireless communications.

Acknowledgements

This work was supported in part by the Ministerio de Ciencia, Innovación y Universidades under the project TEC2017-86619-R (ARTEINE); by the Ministerio de Economía, Industria y Competitividad under the project TEC2016-75103-C2-1-R (MYRADA); by the Gobierno del Principado de Asturias/FEDER under the project GRUPIN-IDI/2018/000191; by the Gobierno del Principado de Asturias through the Programa “Clarín” de Ayudas Postdoctorales/Marie Curie COFUND under the project ACA17-09; and by Ministerio de Educación, Cultura y Deporte/Programa de Movilidad “Salvador de Madariaga” (Ref. PRX18/00424).

Thanks

The authors would like to thank Dr. R. Florencio, Prof. R. R. Boix and Prof. J. A. Encinar for providing the MoM-LP software for the analysis of the reflectarray cell.

Author details


Daniel Rodríguez Prado¹, Manuel Arrebola^{2*} and Marcos Rodríguez Pino²

¹ Institute of Sensors, Signals and Systems, School of Engineering and Physical Sciences, Heriot-Watt University, Edinburgh, UK

² Department of Electrical Engineering, Group of Signal Theory and Communications, Universidad de Oviedo, Gijón, Spain

*Address all correspondence to: arrebola@uniovi.es

IntechOpen

© 2019 The Author(s). Licensee IntechOpen. This chapter is distributed under the terms of the Creative Commons Attribution License (<http://creativecommons.org/licenses/by/3.0>), which permits unrestricted use, distribution, and reproduction in any medium, provided the original work is properly cited. 

References

- [1] Giambene G, Kota S, Pillai P. Satellite-5G integration: A network perspective. *IEEE Network*. 2018;**32**(5): 25-31
- [2] Imbriale WA, Gao S, Boccia L, editors. *Space Antenna Handbook*. Hoboken, NJ, USA: John Wiley & Sons; 2012
- [3] Bergmann JR, Hasselmann FJV, Pereira LCP, Branco MGC. Reflector antenna configurations for radio base stations in cellular communications. In: *IEEE-APS Conference on Antennas and Propagation for Wireless Communications*. Waltham, Massachusetts, USA; 1998. pp. 61-64
- [4] Berry DG, Malech RG, Kennedy WA. The reflectarray antenna. *IEEE Transactions on Antennas and Propagation*. 1963;**11**(6):645-651
- [5] Huang J, Encinar JA. *Reflectarray Antennas*. Hoboken, NJ, USA: John Wiley & Sons; 2008
- [6] Pozar DM, Metzler TA. Analysis of a reflectarray antenna using microstrip patches of variable size. *Electronics Letters*. 1993;**29**(8):657-658
- [7] Zornoza JA, Encinar JA. Efficient phase-only synthesis of contoured-beam patterns for very large reflectarrays. *International Journal of RF and Microwave Computer-Aided Engineering*. 2004;**14**(5):415-423
- [8] Bucci OM, Franceschetti G, Mazzarella G, Panariello G. Intersection approach to array pattern synthesis. *IEE Proceedings: Microwaves, Antennas and Propagation*. 1990;**137**(6):349-357
- [9] Prado DR, Álvarez J, Arrebola M, Pino MR, Ayestarán RG, Las-Heras F. Efficient, accurate and scalable reflectarray phase-only synthesis based on the Levenberg-Marquardt algorithm. *Applied Computational Electromagnetics Society Journal*. 2015; **30**(12):1246-1255
- [10] Bucci OM, Capozzoli A, D'Elia G, Musto S. A new approach to the power pattern synthesis of reflectarrays. In: *Proc. URSI International Symposium on Electromagnetic Theory (EMTS'04)*. Italy: Pisa; 2004. pp. 1053-1055
- [11] Hasani H, Kamyab M, Ali M. Low cross-polarization reflectarray antenna. *IEEE Transactions on Antennas and Propagation*. 2011;**59**(5):1752-1756
- [12] Tienda C, Encinar JA, Arrebola M, Barba M, Carrasco E. Design manufacturing and test of a dual-reflectarray antenna with improved bandwidth and reduced cross-polarization. *IEEE Transactions on Antennas and Propagation*. 2013;**61**(3): 1180-1190
- [13] Florencio R, Encinar JA, Boix RR, Pérez-Palomino G, Toso G. Cross-polar reduction in reflectarray antennas by means of element rotation. In: *10th European Conference on Antennas and Propagation (EuCAP)*. Davos, Switzerland; 2016. pp. 1-5
- [14] Bucci OM, D'Elia G, Mazzarella G, Panariello G. Antenna pattern synthesis: A new general approach. *Proceedings of the IEEE*. 1994;**82**(3):358-371
- [15] Florencio R, Encinar JA, Boix RR, Losada V, Toso G. Reflectarray antennas for dual polarization and broadband telecom satellite applications. *IEEE Transactions on Antennas and Propagation*. 2015;**63**(4):1234-1246
- [16] Bucci OM, D'Elia G, Romito G. Power synthesis of conformal arrays by a generalised projection method. *IEE Proceedings-Microwaves, Antennas and Propagation*. 1995;**142**(6):467-471

[17] Prado DR, Arrebola M. Effective XPD and XPI optimization in reflectarrays for satellite missions. *IEEE Antennas and Wireless Propagation Letters*. 2018;**17**(10):1856-1860

[18] Florencio R, Boix RR, Encinar JA. Enhanced MoM analysis of the scattering by periodic strip gratings in multilayered substrates. *IEEE Transactions on Antennas and Propagation*. 2013;**61**(10):5088-5099

[19] Zhou M, Sørensen SB, Kim OS, Jørgensen E, Meincke P, Breinbjerg O. Direct optimization of printed reflectarrays for contoured beam satellite antenna applications. *IEEE Transactions on Antennas and Propagation*. 2013;**61**(4):1995-2004

[20] Prado DR, Arrebola M, Pino MR, Florencio R, Boix RR, Encinar JA, et al. Efficient crosspolar optimization of shaped-beam dual-polarized reflectarrays using full-wave analysis for the antenna element characterization. *IEEE Transactions on Antennas and Propagation*. 2017;**65**(2):623-635

[21] Carrasco E, Arrebola M, Encinar JA, Barba M. Demonstration of a shaped beam reflectarray using aperture-coupled delay lines for LMDS central station antenna. *IEEE Transactions on Antennas and Propagation*. 2008;**56**(10):3103-3111

[22] SES-12's mission. Available from: <https://www.ses.com/our-coverage/satellites/365> [Accessed: 28 August 2019]